Thesis for The Degree of Licentiate of Engineering
in Thermo and Fluid Dynamics

Low head pumped hydro storage with contra-rotating pump-turbines

Jonathan Fahlbeck

Department of Mechanics and Maritime Sciences
CHALMERS UNIVERSITY OF TECHNOLOGY
Gothenburg, Sweden, 2022

Low head pumped hydro storage with contra-rotating pump-turbines

Jonathan Fahlbeck

Thesis for The Degree of Licentiate of Engineering No. 2022:08

Department of Mechanics and Maritime Sciences
Division of Fluid Dynamics
Chalmers University of Technology
SE-412 96 Göteborg,
Sweden
Phone: +46(0)31 772 1000

Printed by Chalmers Digitaltryck,
Gothenburg, Sweden 2022.

Low head pumped hydro storage with contra-rotating pump-turbines

Jonathan Fahlbeck

Department of Mechanics and Maritime Sciences
Division of Fluid Dynamics
Chalmers University of Technology

Abstract

The increasing share of electrical energy production by intermittent sources pushes the demand for energy storage. Pumped hydro storage (PHS) has a long history of providing a cost-efficient energy storage solution. However, for PHS to be a viable option, a large head is typically required. This makes energy storage via PHS difficult in countries that lack high mountain regions. To address this problem, and thus allow for PHS in flat countries, the EU project ALPHEUS was formed. In ALPHEUS, new pump-turbine technologies intended for low head PHS are evaluated. One of the investigated designs is a shaft-driven contra-rotating pump-turbine (CRPT). In this thesis, CRPTs are numerically simulated with computational fluid dynamics at stationary and transient operating conditions. The stationary operation is studied through both steady-state and unsteady simulations. The steady-state computations are made to get an understanding of the operating range of the CRPT. The unsteady simulations are carried out on selected operating points with the aim to identify the complex flow behaviour. The transient operations cover startup and shutdown procedures in both pump and turbine modes. The pump mode startup procedure is the major focus since it was found when evaluating preliminary startup and shutdown sequences that the pump mode startup was exposed to the largest loads. Hence, three parallel studies are presented in this thesis to determine how to startup the CRPT in pump mode and limit high-amplitude load variations. This contributes to the machine's lifetime and flexible operation. The outcome of this research shows the potential of using CRPTs in a low head PHS situation and may also help with solving the inherent problems correlated to energy production from intermittent sources.

Keywords

Pumped hydro storage, Hydropower, Low head, Contra-rotating, Pump-turbine, Energy storage, CFD, OpenFOAM, Transients

Acknowledgements

First and foremost, I would like to thank my two supervisors Håkan Nilsson and Saeed Salehi. Our countless discussions and the amount of constructive feedback have constantly kept me going forward and developing as a researcher. Furthermore, I would like to thank all colleagues and staff at the Department of Mechanics and Maritime Sciences, Division of Fluid Dynamics, at Chalmers University of Technology.

I would also like to acknowledge the ALPHEUS, EU Horizon 2020, project with grant agreement No. 883553, for financing my research. From the ALPHEUS project, I would especially like to thank Ruben Ansorena-Ruiz, Justus Hoffstädt, Luiz Gans, Daan Truijen, Melvin Joseph, Mehrdad Zangeneh and Jeremy Bricker. I am delightedly for all our constructive meetings and frictionless collaboration. This has for sure enabled the stable progress of the ALPHEUS project.

I am thanking the Swedish National Infrastructure for Computing (SNIC) at NSC and C3SE, partially funded by the Swedish Research Council through grant agreement No. 2018-05973, for providing computational resources. Without your computer clusters, the numerical simulations made in my research would not have been possible.

Last but not the least, I am more than grateful over my wonderful fiancée Gudrun Dovner. Thank you for showing such a great interest in what I work with, and for all the fantastic questions you ask when we talk about my research or when you read my articles.

Jonathan Fahlbeck
Gothenburg, October 2022

Nomenclature

Acronyms

ALPHEUS	Augmenting grid stability through low head pumped hydro energy utilization and storage
AMI	Arbitrary mesh interface
CD	Central difference
CFD	Computational fluid dynamics
CRPT	Contra-rotating pump-turbine
GGI	General grid interface
LU	Linear-upwind
LUST	Linear-upwind stabilised transport
PHS	Pumped hydro storage
RANS	Reynolds-averaged Navier-Stokes
SAS	Scale adaptive simulation
SST	Shear stress transport
VL	Velocity line

English symbols

$\boldsymbol{n}$	Normal vector	–
$\boldsymbol{S}_\mathrm{f}$	Face area normal vector	m^2
A	Area	m^2
d	Diameter	m
F	Force	N
g	Gravitational acceleration	$\mathrm{m/s}^2$
H	Head	m
k	Turbulent kinetic energy	$\mathrm{m}^2/\mathrm{s}^2$
k_V	Valve minor loss coefficient	–
L	Length or Length scale	m
$N_{\mathrm{R}i}$	Runner rotational speed	rpm
P	Power	W
p	Pressure	$\mathrm{kg}/(\mathrm{m}\cdot\mathrm{s}^2)$
Q	Volumetric flow rate	m^3/s
T	Torque	$\mathrm{N}\cdot\mathrm{m}$
t	Time	s
u	Velocity	m/s

Greek symbols

α_V	Valve opening	$^\circ$
η	Efficiency	%
ν	Fluid kinematic viscosity	m^2/s
Ω	Runner rotational speed	rad/s
ω	Specific rate of dissipation	$1/s$
ϕ	Arbitrary quantity	$-$
ρ	Fluid density	kg/m^3
x	Spatial direction	m

Subscripts

θ	Tangential direction
r	Radial direction
z	Axial direction
a	Absolute
BC	Boundary condition
d	Downstream
f	Face or Friction loss
Far	Location far from boundary
m	Minor loss
r	Relative
R1	Runner 1
R2	Runner 2
t	Turbulent
u	Upstream

List of publications

Appended publications

This thesis is based on the following publications:

Paper A J. Fahlbeck, H. Nilsson, S. Salehi, M. Zangeneh, M. Joseph, Numerical analysis of an initial design of a counter-rotating pump-turbine, *IOP Conference Series: Earth and Environmental Science* **774** (1) (2021) p. 012066. DOI: 10.1088/1755-1315/774/1/012066

Paper B J. Fahlbeck, H. Nilsson, S. Salehi, Flow Characteristics of Preliminary Shutdown and Startup Sequences for a Model Counter-Rotating Pump-Turbine, *Energies* **14** (12) (2021) p. 3593.
DOI: 10.3390/en14123593

Paper C J. Fahlbeck, H. Nilsson, S. Salehi, A Head Loss Pressure Boundary Condition for Hydraulic Systems, *OpenFOAM Journal* **2** (2022) pp. 1–12.
DOI: 10.51560/ofj.v2.69

Paper D J. Fahlbeck, H. Nilsson, S. Salehi, Evaluation of startup time for a model contra-rotating pump-turbine in pump-mode, *IOP Conference Series: Earth and Environmental Science*, accepted awaiting publication.

Paper E J. Fahlbeck, H. Nilsson, S. Salehi, Surrogate based optimisation of a pump mode startup sequence for a contra-rotating pump-turbine using a genetic algorithm and computational fluid dynamics, *Submitted for journal publication*, under review.

Other publications

The following relevant publications are authored or co-authored by Jonathan Fahlbeck. However, they are not appended to, or part of, this thesis.

Paper I L. Uppström, J. Fahlbeck, E. Lillberg, H. Nilsson, Simulation of a shut-down transient in the Francis-99 turbine model, *IOP Conference Series: Earth and Environmental Science* **405** (1) (2019) p. 012026. DOI: 10.1088/1755-1315/405/1/012026

Paper II M. Qudaih, B. Engel, D.P.K. Truijen, J.D.M. De Kooning, K. Stockman, J.P. Hoffstaedt, A.J. Laguna, R. Ansorena-Ruiz, N. Goseberg, J.D. Bricker, J. Fahlbeck, H. Nilsson, L. Bossi, M. Joseph, and M. Zangeneh, The Contribution of Low-Head Pumped Hydro Storage to a Successful Energy Transition, *Proceedings of the Virtual 19th Wind Integration Workshop* (2020).

Paper III J.P. Hoffstaedt, D.P.K. Truijen, J. Fahlbeck, L.H.A. Gans, M. Qudaih, A.J. Laguna, J.D.M. De Kooning, K. Stockman, H. Nilsson, P.T. Storli, B. Engel, M. Marence, J.D. Bricker, Low-head pumped hydro storage: A review of applicable technologies for design, grid integration, control and modelling, *Renewable and Sustainable Energy Reviews* **158** (2022) p. 112119. DOI: 10.1016/j.rser.2022.112119

Paper IV H. Adebi, C.I Uribe, J. Fahlbeck, H. Nilsson, Development of Blade Element Momentum (BEM) Method for Hydropower, *IOP Conference Series: Earth and Environmental Science*, accepted awaiting publication.

Contents

Extended summary

Chapter 1

Introduction

Our current lifestyle results in global warming caused by greenhouse gas emissions [1]. One of the solutions to reduce those emissions is to increase the usage of renewable sources of energy, e.g. wind and solar, for the production of electrical energy [2]. However, the generated electrical energy from these types of renewable sources varies over time due to changes in weather conditions and sunlight. An alternative to compensate for the inherent variation in energy production from intermittent energy sources is the usage of energy storage through hydropower. This technology is commonly referred to as pumped hydro storage (PHS). PHS was in the year 2020 responsible for 90.3% of the power capacity of the world's energy storage [3], which was equivalent to a total power of 160 GW [4]. IRENA [2] stated in 2020 that the installed capacity of PHS needs to be doubled by the year 2050 to 325 GW. This is to cope with the rising intermittent energy source, needed to keep global warming well below 2°C. Between the years 2020 and 2021, the globally installed PHS capacity increased by 3.3% [5]. This shows that PHS is on the right track to align with the rising demands of energy storage.

A typical PHS facility consists of at least two large water reservoirs located at different height elevations (head). The reservoirs are connected via pipelines to move water between them. Potential energy is stored via pumping water from the lower to the upper reservoir [6]. Kinetic energy is utilised by releasing water from the upper to the lower reservoir through a turbine which is connected to a generator. The total energy efficiency of PHS usually varies around 70–80% for various sites [7]. A single unit reversible pump-turbine has been the most popular configuration for pumps and turbines within PHS since the 1950s [8]. The historical development of PHS has primarily focused on site locations where there is a large difference in height elevations between the reservoirs. The main reason for this is due to that the available power and storage capacity is a function of head and flow rate [9]. Thus, with a higher head, a lower flow rate is required, which also leads to a smaller size of the reservoirs. On the other hand, high head PHS is not possible to construct in areas with flat topography [10].

The EU Horizon 2020 project ALPHEUS (Augmenting grid stability through

low head pumped hydro energy utilization and storage) [11], [12] is a research project with the aim to develop energy storage solutions with PHS for low head to ultra-low head (2–20 m) scenarios. Within the ALPHEUS project, three different runner configurations are investigated during the course of the project. Two of the concepts are axial flow pump-turbines with two contra-rotating runners. The difference between the contra-rotating concepts is that one is shaft-driven, and the other is rim-driven. The third concept investigated in ALPHEUS is a positive displacement pump-turbine. All three concepts strive towards round-trip efficiencies of 70–80%. The two contra-rotating alternatives should aim at a design power output of about 10 MW. Furthermore, the final designs should be scalable to cope with local requirements of potential future PHS stations. Besides the round-trip efficiency of the pump-turbines, fatigue and fish friendliness are also considered by the ALPHEUS project.

The ALPHEUS project additionally assesses environmental, economic, and civil engineering aspects of low head PHS. For instance, dam construction and novel powerhouse designs are examined. Also, the potential to exploit offshore energy islands with pump-turbine units [13] in the North Sea are investigated. In addition, new motor/generator designs are investigated for the different runner concepts, as well as power take-off and grid integration. To evaluate the runner designs and power take-off system, experimental tests will be made as part of the ALPHEUS project on a model scale shaft-driven contra-rotating pump-turbine (CRPT) and the positive displacement pump-turbine. Experimental tests of the positive displacement pump-turbine have already been carried out. However, because of the Covid-19 pandemic, the CRPT tests were delayed and not made at the time of writing.

The bulk work of this thesis focuses on analysing the fluid flow of different model scale alternatives of the shaft-driven CRPT with numerical computational fluid dynamics (CFD) simulations. The CRPT is analysed both at stationary operating conditions as well as transient operations. All the numerical simulations are carried out using various versions of the OpenFOAM open-source CFD code [14].

The CRPT configuration is deemed as a promising runner design for low head scenarios due to a number of reasons. To start, an axial flow machine is preferable for a high-power, low head scenario. This is because an axial flow machine works better at higher flow rates and specific speeds compared to centrifugal, or mixed flow, machines [15]. The low head configuration drives the flow rate up since the theoretical power for a hydropower plant is proportional to the volumetric flow rate and the head [16]. Thus, a lower head means a higher flow rate in order to achieve higher power. However, the axial flow requirement can readily be achieved with a single runner configuration. The main advantage of using a CRPT instead of a single runner is that it can be of smaller size and have a wider range of high efficiency with independent speed control of the runners [17]. However, the disadvantages of a CRPT are that it requires a more complex shaft and motor/generator alignment and presents a more complex flow field due to rotor-rotor interaction.

Chapter 2

Theory and methodology

The CRPT is numerically analysed using CFD at stationary and transient conditions. Therefore, the basic workflow of the CRPT is first discussed in Section 2.1. This is followed by a description of the various model scale numerical geometries used with the CRPT in Section 2.2. Finally, the governing equations and numerical framework is presented in Section 2.3.

2.1 Working principles of the contra-rotating pump-turbine

The general mechanism of the contra-rotating pump-turbine is depicted by the velocity triangles in Fig. 2.1. Starting with the turbine mode (dashed arrows), water from an upper reservoir flow over the runner blade surfaces, which creates a pressure and a suction side on the runner blades. The pressure difference between the runner blade surfaces makes the runner rotate. According to Newton's third law, when the runner rotates in a clockwise direction due to the flow, the flow must exhibit an equally strong angular momentum in the

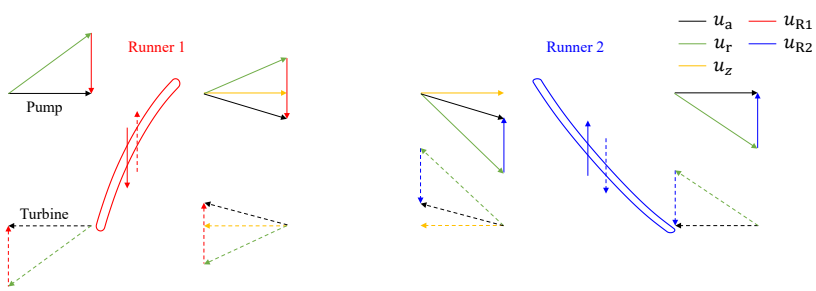

Figure 2.1: Velocity triangles for the CRPT in pump mode (solid lines) and turbine mode (dashed lines). The subscripts a is for absolute, r is for relative, z is the axial direction (positive in pump mode, and negative in turbine mode), R1 is for Runner 1, and R2 is for Runner 2.

anti-clockwise direction. The angular momentum transferred from the flow to the runner is used as the torque to drive a generator to produce electrical energy.

The change of angular momentum over Runner 2 (upstream in turbine mode) introduces a swirl component to the flow in an anti-clockwise direction between the runners. The basic mechanism that makes Runner 2 rotate is the same as the one that makes Runner 1 rotate. The main difference is that Runner 1 is designed to de-swirl the flow, making the flow close to axial after the runner.

In pump mode (solid lines in Fig. 2.1), the flow is from left to right and the rotational directions of the runners are shifted. In contrast to turbine mode, a pump needs to create a sufficient pressure increase, usually referred to as the net head, to drive the flow from a lower to an upper reservoir. This is achieved by angular momentum being added to the flow via electric motors that transfer torque, which makes the runners rotate. The added angular momentum to the flow over Runner 1 (upstream in pump mode) results in a clockwise swirl component to the flow, as shown in Fig. 2.1. Just as in turbine mode, the CRPT is designed to de-swirl the rotating flow component over the downstream Runner 2, making the flow close to axial after Runner 2.

The terms contra-rotating and counter-rotating are within the hydropower research community used rather frequently while referring to the same configuration. The same is also true for the author of this thesis. In my earlier publications, I used the term counter-rotating, while in the later works the term contra-rotating is used. The reason for this is that, within aeronautical propulsion systems, contra-rotating means two propellers fitted on a coaxial shaft, rotating in opposite directions. However, the term counter-rotating is used for twin-, or multi-engine, aircrafts where the propeller(s) on each side of the aircraft rotate in opposite directions. Hence, the term contra-rotating is more in line with what is used in other industries for the type of pump-turbine configuration investigated within this thesis.

2.2 Geometries and numerical domains

A number of different numerical domains have been used for the transient CFD computations, and they are illustrated in Fig. 2.2. In common for the displayed domains, Runner 1 is in red, Runner 2 is in blue, and a mounting arrangement with support structures is included. The concept with the mounting arrangement is that the runners are connected to motors/generators via individual shafts that go inside the hub and a support-strut (see Fig. 3.2). The various domains were derived and changed based on the layout of a future experimental test facility, where a model scale CRPT is planned to be tested. The top geometry is an early draft and was used in the studies presented in Papers A and B. In that geometry, a runner diameter of 270 mm was assumed. The middle domain is a refined version of the top domain and includes an extended straight section by the runners, and uses a runner diameter of 276 mm. The middle domain was used in Papers D and E, and Section 3.3. The bottom domain

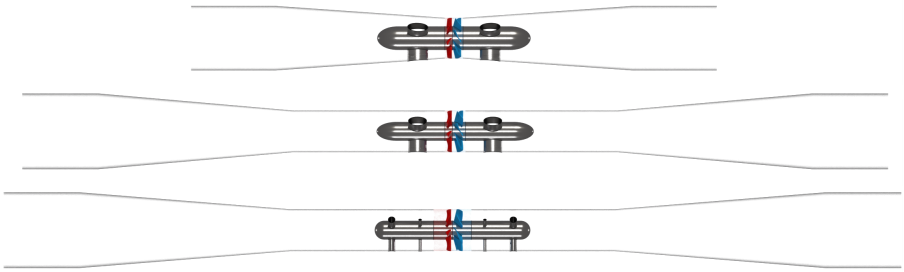

Figure 2.2: Numerical domains used for the unsteady and transient studies

is the geometry that is currently planned to be used in the test facility and some results using this geometry are presented in Section 3.4. The differences between the bottom domain and the middle domain are that the hub shape is changed, the runner diameter is slightly increased to 277 mm, and two sets of additional support struts are present. Furthermore, the cone angle of the contraction/expansion parts is marginally reduced.

For the steady-state computations presented in Section 3.5, a single blade-passage (stage) approached was used. In the single blade-passage, only one runner blade per runner was included in the simulation. To model the presence of the full runners, cyclic boundaries were used.

2.3 Computational fluid dynamics modelling

The numerical CFD simulations carried out within this work are made with the OpenFOAM open-source CFD code [14]. Different versions of OpenFOAM have been used through the project, but OpenFOAM-v1912 [18] and v2012 [19] have extensively been used for the unsteady and transient computations. Foam-extend 4.1 nextRelease branch has been used for the steady-state computations since it contains a mixing-plane interface. Other versions of OpenFOAM currently lack a mixing-plane implementation.

2.3.1 Governing equations

The incompressible Reynolds-averaged Navier-Stokes (RANS) equations are used for the numerical CFD computations. The RANS equations read

$$\frac{\partial \bar{u}_i}{\partial x_i} = 0, \tag{2.1}$$

and

$$\underbrace{\frac{\partial \bar{u}_i}{\partial t}}_{\text{temporal}} + \underbrace{\frac{\partial \bar{u}_i \bar{u}_j}{\partial x_j}}_{\text{convection}} = \underbrace{-\frac{1}{\rho}\frac{\partial \bar{p}}{\partial x_i}}_{\text{source}} + \underbrace{\frac{\partial \bar{u}_i}{\partial x_j}\left(\nu \frac{\partial \bar{u}_i}{\partial x_j} - \overline{u_i' u_j'}\right)}_{\text{diffusion}}, \tag{2.2}$$

for continuity and momentum in tensorial notation, respectively. In the equations, u is the velocity, x is the spatial direction, p is the pressure, ρ is the

fluid density, and ν is the fluid kinematic viscosity. The overline symbol '$^-$' denotes that the quantity is time-average. The unknown Reynolds stress tensor (divided by the density) $\overline{u_i' u_j'}$ is modelled through Boussinesq's assumption, which states

$$\overline{u_i' u_j'} = -\nu_\mathrm{t} \left(\frac{\partial \bar{u}_i}{\partial x_j} + \frac{\partial \bar{u}_j}{\partial x_i} \right) + \frac{2}{3} \delta_{ij} k. \tag{2.3}$$

Here ν_t is the turbulent kinematic viscosity, k is the turbulent kinetic energy and δ_{ij} is the Kronecker delta.

For closure of the RANS equations (Eq. (2.1) and Eq. (2.2)) the k-ω SST-SAS (shear stress transport - scale adaptive simulation) turbulence model is used for the unsteady simulations. The regular k-ω SST model is used for the steady-state simulations. The turbulent kinetic energy is defined as $k = 0.5\overline{u_i' u_i'}$, and the turbulent kinematic viscosity as $\nu_\mathrm{t} = \frac{\beta^{*1/2} k}{\max(\beta^{*1/2}\omega, S F_2)}$ in the turbulence models. The k-equation reads

$$\frac{\partial k}{\partial t} + \bar{u}_j \frac{\partial k}{\partial x_j} = P_k - \beta^* k\omega + \frac{\partial}{\partial x_j} \left[(\nu + \sigma_k \nu_\mathrm{t}) \frac{\partial k}{\partial x_j} \right], \tag{2.4}$$

and the specific rate of dissipation (ω) SST equation is

$$\frac{\partial \omega}{\partial t} + \bar{u}_j \frac{\partial \omega}{\partial x_j} = P_\omega - \beta \omega^2 + \frac{\partial}{\partial x_j} \left[(\nu + \sigma_\omega \nu_\mathrm{t}) \frac{\partial \omega}{\partial x_j} \right] + 2(1 - F_1) \sigma_{\omega 2} \frac{1}{\omega} \frac{\partial k}{\partial x_j} \frac{\partial \omega}{\partial x_j}. \tag{2.5}$$

The model coefficients and functions are according to Menter [20].

The SAS modifications to the SST model are made by introducing an additional source term, Q_SAS, into the ω-equation [21]–[23]. In OpenFOAM-v2012 the Q_SAS term reads [22]

$$Q_\mathrm{SAS} = \max \left[\zeta_2 \kappa S^2 \left(\frac{L}{L_\mathrm{vK}} \right)^2 - C \frac{2k}{\sigma_\Phi} \max \left(\frac{|\nabla \omega|^2}{\omega^2}, \frac{|\nabla k|^2}{k^2} \right), 0 \right]. \tag{2.6}$$

Here L_vK is the von Karman length scale which is defined as $\kappa |\boldsymbol{U}'/\boldsymbol{U}''|$. The first velocity derivative ($\boldsymbol{U}'$) is expressed as $S = \sqrt{2 \bar{s}_{ij} \bar{s}_{ij}}$, where $\bar{s}_{ij} = 0.5(\partial \bar{u}_i/\partial x_j + \partial \bar{u}_j/\partial x_i)$. The second velocity derivative ($\boldsymbol{U}''$) is described as $|\nabla^2 \boldsymbol{u}|$. This results in that $L_\mathrm{vK} = \kappa S/|\nabla^2 \boldsymbol{u}|$. The OpenFOAM-v2012 implementation of the von Karman length scale includes dampening of the smallest resolved turbulent fluctuations and reads [22]

$$L_\mathrm{vK} = \max \left(\frac{\kappa S}{|\nabla^2 \boldsymbol{u}|}, C_\mathrm{s} \sqrt{\frac{\kappa \zeta_2}{\beta/\beta^* - \alpha}} \Delta \right). \tag{2.7}$$

Here Δ is the filter width (cubic root of the cell volume). All model coefficients and functions are found in the works by Menter and Egorov [21]–[23].

2.3.2 Discretisation schemes

The RANS equations and turbulent quantities are discretised and solved for on a computational mesh. The choice of selecting numerical discretisation schemes is often a trade-off between stability and accuracy of the simulation. In this work, no formal studies have been carried out to find the most appropriate sets of schemes. Instead, the selection is based on experience by the author and within the research group.

For a control volume, the general transport equation of an arbitrary scalar ϕ, and applying Gauss divergence theorem ($\int_V \nabla\phi \, \mathrm{d}V = \int_A \phi \cdot \boldsymbol{n} \, \mathrm{d}A$) is defined as [24]

$$\underbrace{\frac{\partial}{\partial t}\int_{\mathrm{V}} \phi \, \mathrm{d}V}_{\text{temporal}} + \underbrace{\int_A (\phi \boldsymbol{u}) \cdot \boldsymbol{n} \, \mathrm{d}A}_{\text{convection}} = \underbrace{\int_A (\Gamma \nabla \phi) \cdot \boldsymbol{n} \, \mathrm{d}A}_{\text{diffusion}} + \underbrace{\int_{\mathrm{V}} S_\phi \, \mathrm{d}V}_{\text{source}}. \tag{2.8}$$

In the equation, V is the volume of the control volume, A is the area/surface of the control volume, $\boldsymbol{n}$ is the area/surface normal, Γ is the diffusion coefficient, and S_ϕ represent source term(s).

Temporal

The discretisation of time is for the unsteady simulations handled with the backward scheme [25]. The backward scheme is second-order accurate, and the temporal derivative is approximated as

$$\frac{\partial \phi}{\partial t} = \frac{\frac{3}{2}\phi^n - 2\phi^o + \frac{1}{2}\phi^{oo}}{\Delta t}. \tag{2.9}$$

The scheme uses three time instances, which are $\phi(t + \Delta t) = \phi^n$, $\phi(t) = \phi^o$, and $\phi(t - \Delta t) = \phi^{oo}$. A number of publications have been made where the backward scheme is used for Francis and Kaplan turbines and the results have been validated against experimental data [26]–[28].

In all simulations carried out, a fixed time step is employed. The length of the time step varies with case and fidelity of the CFD model used for the various studies. The maximum runner rotation per time-step is between 0.25–2.25° in the simulations.

Convection

The convection term in Eq. (2.8) can be reformulated on a computational mesh to sum all fluxes on the surfaces of a computational cell as

$$\int_A (\phi \boldsymbol{u}) \cdot \boldsymbol{n} \, \mathrm{d}A = \sum_f (\phi \boldsymbol{u})_\mathrm{f} \cdot \boldsymbol{S}_\mathrm{f}, \tag{2.10}$$

where $\boldsymbol{S}_\mathrm{f}$ is the face area normal vector. In OpenFOAM, the volumetric face flux $(\boldsymbol{u} \cdot \boldsymbol{S})_\mathrm{f}$ is calculated and stored as a variable, here denoted $\Phi = (\boldsymbol{u} \cdot \boldsymbol{S})_\mathrm{f}$ [26]. However, the face value of the transported variable ϕ_f is determined by interpolation.

Convection terms of the turbulent kinetic energy and the specific rate of dissipation are managed with the first order upwind scheme for stability reasons. With the first order upwind scheme, the face value ϕ_f is assumed to equal the cell centre value ϕ_c from the upwind cell [25].

The convection terms of the three velocity components are discretised with the LUST (linear-upwind stabilised transport) scheme [29]. The LUST scheme is a blend scheme that combines a central difference (CD) scheme for accuracy and a linear upwind (LU) scheme for stability. The LUST scheme is defined as

$$\phi_{\mathrm{f,LUST}} = \gamma\phi_{\mathrm{f,LU}} + (1-\gamma)\phi_{\mathrm{f,CD}}, \tag{2.11}$$

where γ is a linear weight equal to 0.25 in OpenFOAM. Thus, LUST uses 25% of the linear upwind scheme

$$\phi_{\mathrm{f,LU}} = \phi_\mathrm{u} + (\boldsymbol{x}_\mathrm{f} - \boldsymbol{x}_\mathrm{u})\nabla_\mathrm{u}\phi, \tag{2.12}$$

and 75% of the central difference scheme

$$\phi_{\mathrm{f,CD}} = \lambda\phi_\mathrm{u} + (1-\lambda)\phi_\mathrm{d}, \quad \text{where} \quad \lambda = \frac{|\boldsymbol{x}_\mathrm{d} - \boldsymbol{x}_\mathrm{f}|}{|\boldsymbol{x}_\mathrm{d} - \boldsymbol{x}_\mathrm{u}|}. \tag{2.13}$$

The subscripts u and d are for upwind and downwind cell centres, respectively. The term $\nabla_\mathrm{u}\phi$ is the cell centre gradient at the upwind cell, and $\boldsymbol{x}$ is the spatial position of a cell or face centre.

Convection terms of all other variables in the numerical simulations are handled with the central difference scheme, Eq. (2.13).

Diffusion, gradient and interpolation

Numerical schemes for the diffusion terms, or laplacian schemes as they are called in OpenFOAM, are formulated similarly as the convection terms as

$$\int_A (\Gamma\nabla\phi)\cdot\boldsymbol{n}\ \mathrm{d}A = \sum_f (\Gamma\nabla\phi)_\mathrm{f}\cdot\boldsymbol{S}_\mathrm{f}. \tag{2.14}$$

In the computations, the central difference scheme is used without any additional corrections.

The pressure gradient in Eq. (2.2) is a typical example of a source term. For all gradient terms, the central difference scheme is used without any corrections. Likewise, interpolation terms are managed with the central difference scheme.

2.3.3 Mesh interfaces

The used numerical domains in Section 2.2 are decomposed into different mesh regions. To connect the mesh regions, sliding mesh interfaces with the arbitrary mesh interface (AMI) [30], [31] technique is used in the unsteady computations in OpenFOAM-v1912 and v2012. The AMI uses a conservative interpolation approach to transfer fluxes between neighbouring mesh regions with non-conformal mesh connectivity.

For the steady-state computations made in foam-extend 4.1 nextRelease branch, mixing-plane and cyclic-GGI (general grid interface) interfaces are used to mimic the full rotating runners. The mixing-plane interface uses tangential averaging at various radial positions [32] and it is within this thesis used for single blade rotor-rotor coupling. The cyclic-GGI provides a cyclic boundary condition, which allows that only a single blade for each runner is needed in the steady-state simulations.

2.3.4 Pressure and velocity coupling in OpenFOAM

For the steady-state computations, the SIMPLE algorithm [33] is used to couple pressure and velocity with the incompressible `MRFSimpleFoam` solver in foam-extend 4.1 nextRelease branch. For the unsteady and transient computations in OpenFOAM-v1912 and v2012, the `pimpleFoam` solver is used. The `pimpleFoam` solver is an incompressible solver that uses the PIMPLE algorithm [34], [35] to establish a pressure–velocity coupling. The PIMPLE algorithm combines the SIMPLE and the PISO [36] algorithms. Fig. 2.3 demonstrates the iterative solution procedure of the PIMPLE algorithm. PISO is used as an inner loop corrector step, and SIMPLE as an outer loop.

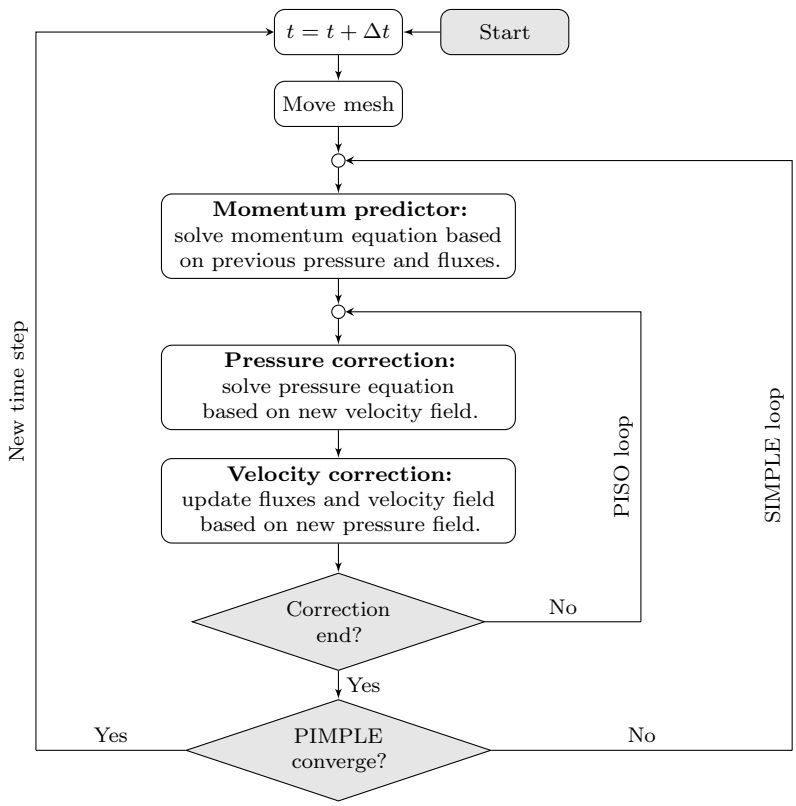

Figure 2.3: Flow chart of the PIMPLE algorithm [34], [35]

Chapter 3

Numerical simulations

The scope of the CFD simulations gradually changes. For this reason, some general comments and results from preliminary studies of transients about the mode scale CRPT are first given in Section 3.1, Papers A and B. The outcome of the preliminary studies led to the realisation that the numerical framework needs to take into account a larger hydraulic system. This is to be able to predict a reasonable flow rate at any given operational point. The approach used to consider the effects of the hydraulic system in the CFD simulations is given Section 3.2 and Paper C. Once the hydraulic system is modelled, the alarming pump mode startup sequence is thoroughly analysed in Section 3.3, Papers D and E. Following the transient simulations in pump mode, velocity probing lines for the future experimental test facility are analysed in turbine mode in Section 3.4. Lastly, the performance of the prototype scale CRPT at several stationary operational points are presented in Section 3.5.

3.1 General behaviour and preliminary transients in pump and turbine modes

The CRPT machine produces complex flow patterns already at the design point, which is indicated by the vorticity magnitude in Fig. 3.1 and discussed in Paper A. This is primarily due to that the downstream runner interacts with the wakes of the upstream runner. The wake interactions of the runners lead to pressure oscillations correlated to the blade passing frequency of each runner,

$$f_{\mathrm{b,R}} = \frac{\Omega}{2\pi} N, \tag{3.1}$$

and various linear combinations of the two runners' blade passing frequencies. In the equation, Ω is the rotational speed of a runner in rad/s, and N is the number of runner blades.

During transient operations of the CRPT, such as change of operational point or shutdown and startup procedures, the flow by the runners may undergo drastic changes. These changes can typically include flow separation by the

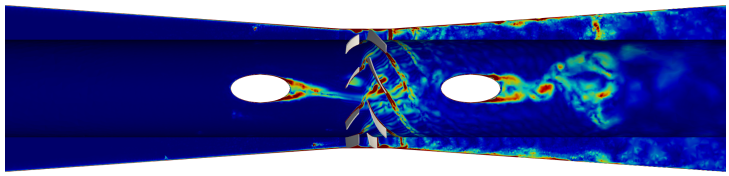

Figure 3.1: Vorticity magnitude displayed on a plane and a cylinder at the design point in pump mode, from Paper B. The flow is from left to right, and it is the top geometry in Fig. 2.2

runner blades, unbalanced torque distribution between the runners or (in pump mode) even flow in the reverse direction. All these phenomena may cause substantial force and torque variations and peaks on the runner blades, which in turn can lead to fatigue or premature breakdown of the CRPT.

A large part of this thesis consists of the startup sequence in pump mode. In Paper B it was shown that the runners exhibit fast and large load (force and torque) variations and reverse flow during a preliminary startup sequence in pump mode. The shutdown procedure also showed high amplitude load values and rapid variations. However, not as severe as the pump mode startup. Fortunately, the turbine mode loads were less substantial than in pump mode.

In Paper B it was argued that a valve needs to be part of the startup and shutdown sequences to prevent reverse flow in pump mode. The flow rate through a hydraulic machine is a balance between the available pressure of the system and the 'used/added' pressure by the machine. Hence, the flow rate and potential risk of reverse flow through the hydraulic system are dependent on the various system components (valves, instruments, etc.) and pipelines. Ideally, the full hydraulic system should be part of the numerical CFD simulations to get the correct flow rate given a specific pressure difference over the system. However, by including the entire hydraulic system in resolved CFD simulations, the computational cost is in a general case today not feasible.

3.2 System modelling and pressure boundary condition

Instead of resolving the full hydraulic system in CFD simulations, the various system components can be modelled as a series of pressure losses. The pressure losses of the system are balanced by the change of pressure over the CRPT at a given flow rate. This led to the development of the `headLossPressure` boundary condition for OpenFOAM, which is presented in Paper C. The basic principle of the `headLossPressure` boundary condition is that Bernoulli's energy equation [37] is applied to the boundaries of the computational domain to update and set the static pressure. For a boundary of the numerical domain, the pressure is calculated as

$$p_{\mathrm{BC}} = p_{\mathrm{Far}} + \frac{\rho}{2}\left(u_{\mathrm{Far}}^2 - u_{\mathrm{BC}}^2\right) + \rho g(z_{\mathrm{Far}} - z_{\mathrm{BC}}) \pm (\Delta p_{\mathrm{m,Far}} + \Delta p_{\mathrm{f,Far}}) \quad (3.2)$$

Here u is the velocity, ρ is the fluid density, g is the gravitational acceleration, z is the location in the direction of the gravitational acceleration, Δp_{m} is pressure losses due to one-time occurrences in the flow path (minor losses), and Δp_{f} is pressure losses caused by friction from the wall (friction losses). Subscripts BC is for boundary condition and 'Far' is a location up or downstream in the hydraulic system. The losses are subtracted if 'Far' is located downstream (inflow boundary) and added if it is upstream (outflow boundary).

The pressure losses due to one-time occurrences in the flow path, Δp_{m}, are usually referred to as minor losses. The minor losses are caused by different sources, such as valves, bends, instruments, etc, and can be characterised by a minor loss coefficient for each of the system components. The minor loss coefficients are typically found as tabulated values, provided by the manufacturer, or estimated with numerical or experimental models. With the developed boundary condition in Paper C, it is further possible to specify a time-varying minor loss coefficient which can be used to model a transient valve sequence.

The sum of pressure losses caused by wall friction, Δp_{f}, is calculated as a function of surface roughness, pipe length and hydraulic diameter, and a friction loss coefficient. The friction loss coefficient is solved iteratively via the Colebrook equation [37].

3.2.1 Hydraulic system

The boundary condition developed in Paper C provides a cost-efficient tool to model a larger hydraulic system of which the CRPT is part. The modelled system is in accordance with the future test facility where the machine is planned to be experimentally evaluated in a mode scale. A schematic view of the future test facility is shown in Fig. 3.2. The test facility consists of upper and lower reservoirs which are connected through pipelines. The head of the lower reservoir can be varied to change the gross head of the facility. Additionally, there is one bend and two valves present in the hydraulic system. One of the valves will be used to regulate the flow rate.

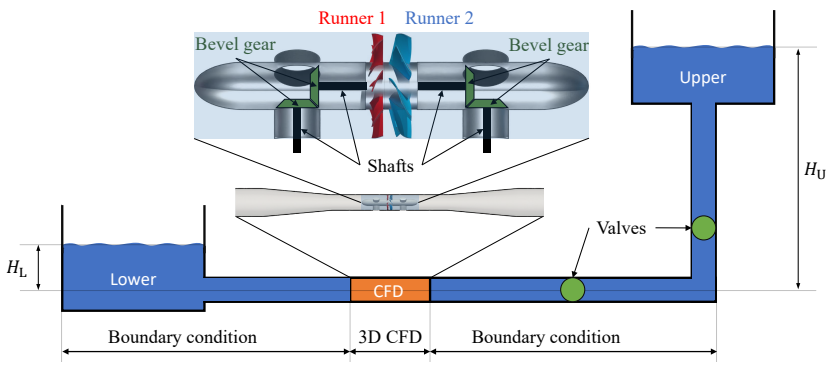

Figure 3.2: Schematic view of the experimental test facility, CFD domain, and conceptual mounting arraignment

Based on experimental data provided by the test facility, a minor loss coefficient of the valve, k_{V}, as a function of valve opening is derived as

$$k_{\mathrm{V}}(\alpha_{\mathrm{V}}) = \exp(-4.2351 \ln(\alpha_{\mathrm{V}}) + 18.1149). \tag{3.3}$$

Here α_{V} is the valve opening in degrees. The exponential function in Eq. (3.3) is compared to the provided experimental test data of the valve in Fig. 3.3. Test data for the valve is only available between valve openings of 10–90°, hence the smaller opening angles are extrapolated based on Eq. (3.3). It is reasonable to assume that the true minor loss coefficient would follow the extrapolated values. This is because the loss coefficient must approach infinity as the valve is closing, and the curve fit shows an excellent agreement with the experimental data for the available opening angles.

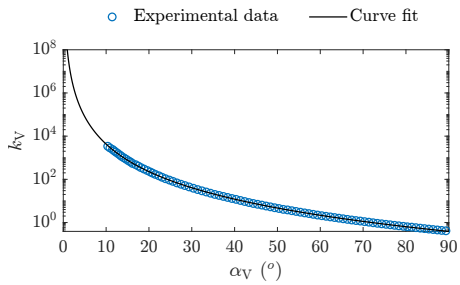

Figure 3.3: Minor loss coefficient of the valve (k_{V}) as a function of valve opening (α_{V}), where 0° is fully closed and 90° is fully open.

3.3 Transient startup sequences in pump mode

In Paper B it was shown that just using the runners to control the startup sequence may result in large force and torque variations. A traditional startup scheme for PHS in pump mode typically includes the speedup of the runner to its nominal rotational speed with a closed valve, or guide vanes [38]. Once the runner has reached its nominal speed and built up sufficient pressure, the valve or guide vanes are slowly opened up. A numerical simulation of such a procedure has been carried out, but not published previously. In that simulation, the schematic hydraulic system shown in Fig. 3.2 is included and a valve sequence is modelled with Eq. (3.3) through the `headLossPressure` boundary condition.

In Fig. 3.4, the computed flow rate, axial forces, and torques are shown for a traditional pump mode startup sequence. In the sequence, the rotational speed of the runners ($N_{\mathrm{R}i}$) is increased from standstill to the nominal rotational speed of 1502 rpm with a fully closed valve between 0.1 and 0.8 s. Subsequently, during the sequence, the valve (α_{V}) is opened between 1 and 4 s. As the valve starts to open, the flow rate (left graph) rapidly increases. The flow rate is at 90% of its final flow rate already at 2.3 s, which is less than half the time of the transient valve opening sequence. By analysing the axial forces (middle

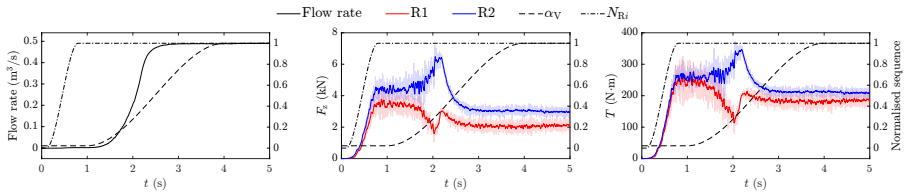

Figure 3.4: Flow rate (left), absolute axial force (middle), and absolute torque (right) as a function of time for the traditional pump mode startup sequence. Normalised sequence on the right axis, a value of 0 is a closed valve (α_V), or no rotational speed (N_{Ri}), a value of 1 is an open valve and a rotational speed of 1502 rpm.

graph) and torques (right graph) of the two runners, it is shown that the general appearance is similar. At roughly 2.1 s, large peak values are noted for Runner 2 (downstream), while Runner 1 (upstream) indicates a drastic decrease in loads. After the peak at 2.1 s, the loads convert to their final values. The load fluctuations are furthermore substantially larger prior to the peak at 2.1 s than after, for both runners. After the load peak, the load fluctuations on Runner 2 show smaller amplitude values compared to Runner 1.

A reason why Runner 2 experience the worst load conditions for the traditional startup sequence is that this runner encounter flow structures leaving the upstream Runner 1. This is seen by the vorticity magnitude in Fig. 3.5 at 2.1 s and 3.5 s. At the earlier time step, the flow field is heavily separated by both the runners, whereas it is more attached at the later time step. With the

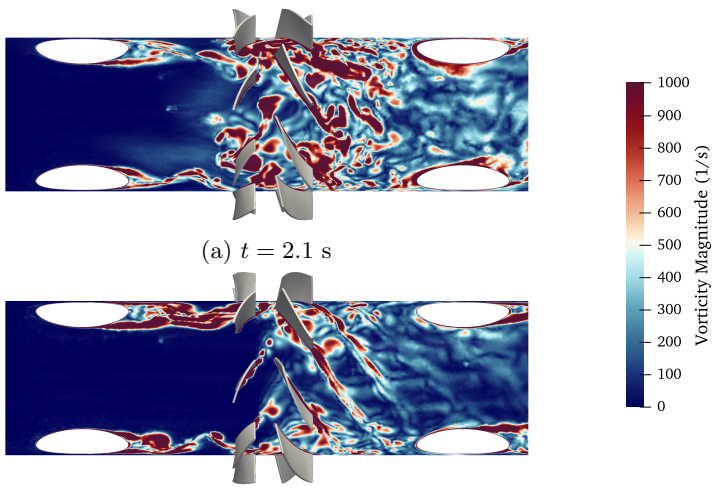

(a) $t = 2.1$ s

(b) $t = 3.5$ s

Figure 3.5: Vorticity magnitude on a cylinder by the runners, at two time steps, for the traditional pump mode startup sequence. Flow from left to right, and it is the middle geometry in Fig. 2.2

traditional sequence (Fig. 3.4) it is clear that there is a tipping point, before and after around 2.1 s. A physical explanation of what is happening is that, as the flow rate increases while opening the valve, the flow is swirled in the direction of Runner 1's rotation between the runners. However, the swirl is in the opposite direction downstream of Runner 2 because of that runner's rotational direction. The drastic change of swirl direction over Runner 2, in combination with the fast acceleration in flow rate, and heavily separated flow field from Runner 1 (c.f. 2.1 s and 3.5 s in Fig. 3.5) causes the high Runner 2 loads at around 2.1 s. As the flow rate continues to reach its final value, the swirl between the runners decreases as a consequence of the increasing flow rate. Furthermore, once the machine reaches its operating point, the upstream flow field of Runner 2 is less severe since the flow is comparably attached to the blade surfaces, as demonstrated in Fig. 3.5.

Because the traditional sequence does not show any more promising results than what is presented in Paper B, the studies in Paper D and Paper E were carried out. The main goal of both studies was to find reasonable alternatives on how to start up the CRPT in pump mode and avoid such high-amplitude loads as demonstrated in Fig. 3.4 and Paper B.

3.4 Stationary operating point in turbine mode

For future lab tests, it is necessary to investigate the velocity profiles at probing lines. This is to get a rough estimate of what type of total pressure probes to be used at the lab and the flow angles. A number of velocity lines (VL) and a contour of velocity magnitude are displayed in Fig. 3.6 at the design point in turbine mode. At velocity line 5 (VL5), which is located upstream in turbine mode, there is a fully developed turbulent flow profile in the negative axial direction (yellow). In the radial (blue) and tangential (red) directions, there is a negligible flow. Downstream of the CRPT at velocity line 1 (VL1), the axial profile shows a fairly symmetric behaviour about the centre line. Effects from the hub are noted at the centre line of the axial profile since the axial velocity is smaller in the centre. A small (negative) tangential velocity is noted by the shroud at VL1. This indicates that there is a small remaining swirl after

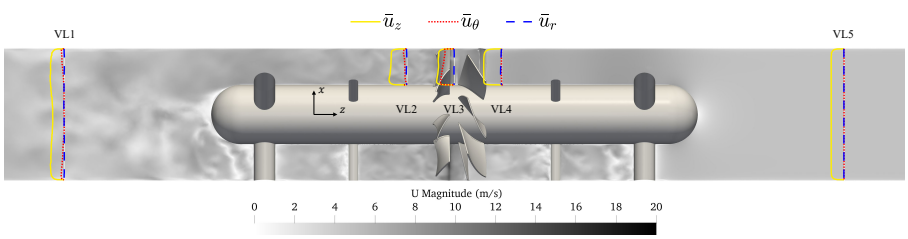

Figure 3.6: Contour of velocity magnitude on a cut plane, and time-averaged velocity profiles at probing lines, at the design point in turbine mode. Flow from right to left, and it is the bottom geometry in Fig. 2.2. Note, negative velocities are in the negative z direction.

the machine. In turbine mode, Runner 2 (upstream) rotates in the positive tangential direction and Runner 1 (downstream) in the negative direction. The negative value of the remaining swirl at VL1 suggests that Runner 1 has not been able to fully de-swirl the flow from Runner 2.

The three velocity lines (VL2–VL4) close to the runners in Fig. 3.6 show the transition that the flow undergoes through the CRPT. The axial velocity at all three lines is considerably larger than at VL1 and VL5. This is because of the decreased cross-sectional area, caused by the hub, which generates an increased axial velocity due to continuity. In fact, the axial profile is fairly constant at VL2–VL4. The same is also true for the radial velocity, which is close to zero. On the other hand, the tangential velocity is transformed from being almost zero at VL4 to having comparably large values at VL3. The increase in negative tangential velocity at VL3 is caused by the change in angular momentum over Runner 2. This is because Runner 2 rotates in the positive tangential direction and the resulting tangential flow velocity between the runners is in the negative tangential direction. Furthermore, the magnitude tangential velocity at VL3 is the largest close to the hub and gradually decreases towards the shroud. After Runner 1 at VL2, the magnitude of the tangential velocity is reduced. However, a small negative tangential velocity component remains at VL2, which is also noted downstream at VL1.

In Fig. 3.7 flow angles between the hub and shroud are shown for VL2–VL4 (see Fig. 3.6). The flow angle is here defined as $\arctan(\bar{u}_\theta/\bar{u}_z)$. Note that the axial velocity is always in the negative z direction in turbine mode. It is important to have a rough estimate of the flow angles for future lab tests since this is a decisive factor when selecting the type of probe. As indicated previously, the tangential velocity is the largest between the runners at VL3. The flow angle at VL3 varies between magnitudes of 30–44°. Before the runners at VL4, there is almost no tangential velocity, which is seen by the close to zero flow angle. However, after the runners at VL2, there is some tangential velocity. The value of the flow angle supports the statement made earlier, that Runner 1 has not been able to de-swirl the flow caused by Runner 2 entirely.

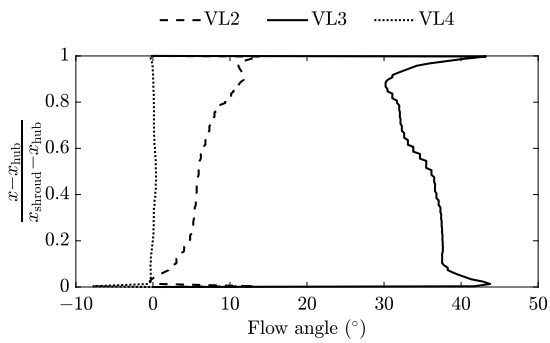

Figure 3.7: Flow angles at the fraction distance between hub and shroud

3.5 Steady-state simulations in prototype scale

Besides all the unsteady and transient computations, a large number of steady-state simulations have been carried out. The aim of the steady-state simulations was to map the performance of the CRPT at various stationary operating points. A few samples of operating points are demonstrated in Paper A. Furthermore, the steady-state data will be used to determine the operating points that are to be evaluated in future lab tests.

Until this point, all demonstrated results have focused on the model scale CRPT. However, from a practical point of view, steady-state simulations of the prototype CPRT have also been carried out. This was first and foremost to be able to design a rigorous control system by other parties of the ALPHEUS project. The initial control system was based on regression models of steady-state CFD data points. Furthermore, one assumed advantage of the CRPT is that the individual runner speeds can be set independently. Hence, it is of interest to investigate the machine at different runner speed ratios. In Fig. 3.8 various runner speed ratios and machine characteristics are demonstrated for the initial prototype scale CRPT.

The machine characteristics in Fig. 3.8 are defined according to Dixon and Hall [16]. The head coefficient,

$$C_{\mathrm{H}} = \frac{gH}{\Omega_{\mathrm{R1}}^2 d^2}, \tag{3.4}$$

the power coefficient,

$$C_{\mathrm{P}} = \frac{P}{\rho \Omega_{\mathrm{R1}}^3 d^5}, \tag{3.5}$$

and the pump and turbine mode efficiencies,

$$\eta_{\mathrm{pump}} = \frac{Q\rho g H}{P}, \quad \eta_{\mathrm{turbine}} = \frac{P}{Q\rho g H}, \tag{3.6}$$

are displayed as a function of the flow coefficient

$$C_{\mathrm{F}} = \frac{Q}{\Omega_{\mathrm{R1}} d^3}. \tag{3.7}$$

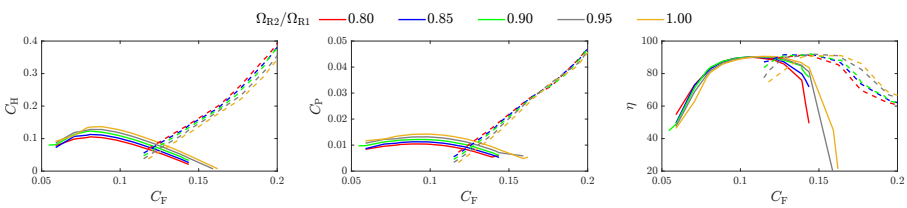

Figure 3.8: Pump and turbine mode characteristics of the initial prototype CRPT at various runner speed rations. Pump mode is indicated with solid lines and turbine mode with dashed lines.

In the equations, g is the gravitational acceleration, H is the net head of the CRPT, Ω_{R1} is the rotational speed of Runner 1, d is the shroud diameter, P is the combined power of the runners, ρ is the fluid density, and Q is the volumetric flow rate. The runner rotational speed ratio is defined as the ratio between the rotational speed of Runner 2 and Runner 1 ($\Omega_{\mathrm{R2}}/\Omega_{\mathrm{R1}}$).

By investigating the curves in Fig. 3.8, it is noted that the characteristics of the CRPT are similar at different speed ratios. Some general trends in the pump mode are that with a higher speed ratio, larger head (left graph) and power (middle graph) coefficients are expected. This is presumably explained by the increase in Runner 2's rotational speed adds more angular momentum to the flow, resulting in a higher power and larger pressure drop (head). In contrast to pump mode, in turbine mode a higher speed ratio results in smaller head and power coefficients. Another observation is that all curves are shifted towards the right with a higher speed ratio, especially by looking at the efficiency (right graph). This suggests that a higher speed ratio is preferable at larger flow rates in relation to the Runner 1 rotational speed.

Chapter 4

Summary of papers

4.1 Paper A

J. Fahlbeck, H. Nilsson, S. Salehi, M. Zangeneh, M. Joseph, Numerical analysis of an initial design of a counter-rotating pump-turbine, *IOP Conference Series: Earth and Environmental Science* **774** (1) (2021) p. 012066. DOI: 10.1088/1755-1315/774/1/012066

Division of work

Original draft written by Fahlbeck. Joseph created the blade geometries and performed the steady-state CFD simulations in CFX. Fahlbeck carried out all simulations in OpenFOAM, both steady-state and unsteady-state computations. All graphs and illustrations were created by Fahlbeck. All authors were responsible for reviewing the manuscript.

Summary and discussion

An initial design of a CRPT, made by Joseph, was analysed using CFD simulations at a number of stationary operating conditions in both pump and turbine modes. The simulations concerned both a prototype scale and a model scale CRPT. In prototype scale, results were compared between the proprietary ANSYS CFX solver and the open-source foam-extend 4.1 nextRelease solver, indicating acceptable agreement between solvers. In model scale, steady-state computations made with foam-extend were compared to unsteady simulations using OpenFOAM-v1912. The results showed that the initial design of the CPRT could achieve hydraulic efficiencies of about 90% in pump and turbine modes. The unsteady simulations were in line with the steady-state at the design point. However, it was made clear that the flow field is rather complex already at the design point due to rotor-rotor interaction.

4.2 Paper B

J. Fahlbeck, H. Nilsson, S. Salehi, Flow Characteristics of Preliminary Shutdown and Startup Sequences for a Model Counter-Rotating Pump-Turbine, *Energies* **14** (12) (2021) p. 3593. DOI: 10.3390/en14123593

Division of work

Original draft written by Fahlbeck. The numerical simulations, post-processing data and creation of graphs were made Fahlbeck. All authors were responsible for reviewing the manuscript.

Summary and discussion

Preliminary shutdown and startup sequences were evaluated using CFD. The sequences were based on the assumption that the flow could be controlled and regulated solely through the rotational speed of the runners. The results showed that the pump mode sequences were more severe than the turbine mode. This was because of that the startup sequence in pump mode demonstrated the largest force and torque variations. Based on the results, it was suggested that a valve should preferably be part of the transient sequences to prevent reverse flow and limit high-amplitude loads during pump mode startup and shutdown.

4.3 Paper C

J. Fahlbeck, H. Nilsson, S. Salehi, A Head Loss Pressure Boundary Condition for Hydraulic Systems, *OpenFOAM Journal* **2** (2022) pp. 1–12.
DOI: 10.51560/ofj.v2.69

Division of work

Original draft written by Fahlbeck. Development of the initial boundary condition, creation of a numerical model, and illustrations were made by Fahlbeck. Nilsson provided a test case and experimental validation data. All authors were responsible for reviewing the manuscript and the code.

Summary and discussion

A new pressure boundary condition for the OpenFOAM open-source CFD code was developed in C++ and validated against available experimental test data. The boundary condition is named `headLossPressure` and has the capabilities to include the main effects from a larger hydraulic system in terms of head/pressure losses for various components (e.g. valve, bends, wall friction, etc.) within the system. The head losses from the system are specified in terms of minor or friction losses. The boundary condition utilises Bernoulli's equation to adjust the pressure at the boundaries of the computational domain. It is possible to specify the head of the system, and time-varying effects e.g. a

transient valve sequence. The results showed that the main pressure variation and computed flow rate were in great agreement with the validation case.

4.4 Paper D

J. Fahlbeck, H. Nilsson, S. Salehi, Evaluation of startup time for a model contra-rotating pump-turbine in pump-mode, *IOP Conference Series: Earth and Environmental Science*, accepted awaiting publication

Division of work

Original draft written by Fahlbeck. The simulations and illustration of results were made by Fahlbeck. All authors were responsible for reviewing the paper.

Summary and discussion

The time of an un-optimised startup sequence in pump mode was evaluated using a low-fidelity CFD model. The startup sequence includes a valve opening and individual speedup of the two runners. In the sequence, it is assumed that the runners were speedup to 61% of their nominal rotational speed with a fully closed valve, this ensured that reverse flow was avoided. In the sequence, the valve first opens, followed by the speedup of the downstream Runner 1 and finally the upstream Runner 2's rotational speed was increased. The `headLossPressure` boundary condition was used to get the main effects from the future experimental test site, and to control the valve opening through a time-varying minor loss coefficient. The results indicated that the low-fidelity CFD model managed to capture the startup sequence adequately when compared to results from a high-fidelity CFD model. When evaluating the time of the startup sequence, it was found that a relatively fast startup time of 10 s would be sufficient if the maximum allowed torque of 250 N·m were to be avoided. A slower startup scheme than 10 s was feasible from a load perspective, however it was showed that not much was gained by increasing the startup time from 20 to 30 s.

4.5 Paper E

J. Fahlbeck, H. Nilsson, S. Salehi, Surrogate based optimisation of a pump mode startup sequence for a contra-rotating pump-turbine using a genetic algorithm and computational fluid dynamics, *Submitted for journal publication*, under review

Division of work

Original draft written by Fahlbeck. The simulations and illustrations were made by Fahlbeck. The optimisation work was made by Fahlbeck. Salehi

made countless suggestions on how to improve the optimisation procedure. All authors were responsible for reviewing the paper.

Summary and discussion

A transient startup sequence in pump mode was optimised using surrogate based optimisation and CFD sample points. The startup sequence was characterised by five design variables, one for the valve and two for each runner. An objective function was derived based on the time integration of the magnitude of the gradient in time of the axial force of both runners. The objective function was mapped onto a Gaussian-process surrogate model as a function of the five design variables. The Gaussian-process surrogate model demonstrated sufficient accuracy with leave-one-out cross validated R^2 and normalised root mean square error values. A genetic elitist algorithm was employed to find an optimal combination of the five design variables to limit low-frequency, high-amplitude loads on the runners. The optimal solution presented drastically reduced load peaks when compared to a baseline case. It was found, that for an optimal startup in pump mode of the CRPT, the valve should open during 73% of the sequence. The downstream Runner 1 should start speeding up prior to that of the upstream Runner 2. The speedup of Runner 1 should occur during most of the sequence, while Runner 2 should speedup in the final third of the sequence.

Chapter 5

Concluding remarks

Low head contra-rotating pump-turbines have been numerically analysed with computational fluid dynamics simulations within this thesis. The current work has primarily focused on numerical simulations of the fluid flow of shaft-driven contra-rotating pump-turbines within the EU Horizon 2020 project ALPHEUS. One of the initial ideas with the ALPHEUS project was that the individual rotational speed of each runner should be used to regulate and control the flow. With this in mind, the preliminary startup and shutdown sequences for both pump and turbine modes were investigated in Paper B. It was found that by only using the runners as a regulator, large force and torque variations were encountered in pump mode. It was hence suggested that a valve needed to be part of the startup and shutdown sequences.

In order to introduce a valve to the simulations, the valve must either be physically part of the numerical domain or modelled. In this work, the valve has been modelled using a time-varying minor loss coefficient of the valve at various opening angles. The valve minor loss coefficient was added to the numerical simulations through the head loss pressure boundary condition, which is described in Paper C. The pressure boundary condition further allowed the various system components of the future experimental test facility to be modelled in the simulations so that a reasonable flow rate could be calculated during the transient simulations.

The results from the traditional startup sequence, evaluated in Section 3.3, suggest that such an operating procedure is not preferable for the contra-rotating pump-turbine for a short valve opening sequence of 3 s. An option to limit the loads is presumably to increase the time of the valve opening, which would be a similar study as the one presented in Paper D. An alternative is to optimise the transient operation, as done in Paper E. By optimising the startup sequence, high-amplitude and low-frequency load oscillations can be limited. If large load oscillations are minimised, the flexibility and lifetime of potential future low head pumped hydro storage stations using contra-rotating pump-turbines may be enhanced.

5.1 Further work

This thesis has merely touched a fraction of what can and needs to be analysed before the contra-rotating pump-turbine is deployed and put into full-scale action. For instance, the current work has not covered any geometrical optimisation or design changes of the runner blade designs. This is because another partner in the ALPHEUS project is focusing on running geometrical optimisation studies of both the shaft-driven and the rim-driven contra-rotating pump-turbines. In future studies, the rim-driven configuration also needs to be analysed under transient operating conditions. Such procedures could be mode switching, startup and shutdown, or change of operating point.

The transient numerical simulations have mainly focused on the pump mode startup sequence of model scale shaft-driven contra-rotating pump-turbines. Further studies on how to optimally operate the machine in both pump and turbine modes under different transient conditions should be carried out. Additionally, unsteady investigations of both stationary and transient operations of the prototype scale machine could be made. Such analysis can also include a thorough frequency analysis of different physical phenomena, for instance, vortex shedding and pressure pulsations to ensure that those do not coincide with the system's natural frequencies.

In the ALPHEUS project, experimental tests are planned to be carried out to generate validation data for the numerical computational fluid dynamics models. Because of the Covid-19 pandemic, the experimental tests were delayed and no validation data was available at the time of writing this thesis. The current plan for the experiments is that they are to take place in the final months of 2022 and the beginning of 2023. Once experimental data is available, the accuracy of the numerical models is to be validated.

Another aspect that has not been thoroughly analysed yet in the ALPHEUS project is the risk of cavitation for the contra-rotating pump-turbine. We have already seen (not presented here or published) in preliminary studies that not all the desired operating points will be reachable for the experimental tests due to the critical risk of cavitation. Thus, cavitation analysis should be carried out in both pump and turbine modes to understand the risk and to get a sense of how much cavitation affects the machine's performance. Such studies could initially be made on the model scale contra-rotating pump-turbine, both numerically and experimentally. The latter should be feasible since the current plan is to install a shroud made of acrylic glass for the runners in the lab tests. This means that it should be possible to visually see cavitating flow during the experimental tests (if there is any). On the other hand, from a practical point of view cavitation also needs to be analysed for the prototype scale to determine the risk and how much the machine must be submerged. No prototype experiments are planned within the bounds of the ALPHEUS project, which means that numerical models need to be used.

Bibliography

[1] IPCC, *Climate Change 2021: The Physical Science Basis. Contribution of Working Group I to the Sixth Assessment Report of the Intergovernmental Panel on Climate Change*. Cambridge University Press, 2021 (cit. on p. 3).

[2] IRENA, *Global Renewables Outlook: Energy Transformation 2050*. International Renewable Energy Agency (IRENA), 2020, ISBN: 978-92-9260-238-3 (cit. on p. 3).

[3] H. E. Murdock, D. Gibb, T. Andre *et al.*, 'Renewables 2021 - Global status report,' France, Tech. Rep. 978-3-948393-03-8, 2021, INIS-FR–21-0788, p. 603 (cit. on p. 3).

[4] IHA, *2021 Hydropower Status Report*. IHA Central Office, London, 2021, URL `https://www.hydropower.org/publications/2021-hydropower-status-report`. (visited on 16th Aug. 2022) (cit. on p. 3).

[5] ——, *2022 Hydropower Status Report*. IHA Central Office, London, 2022, URL `https://www.hydropower.org/publications/2022-hydropower-status-report`. (visited on 16th Aug. 2022) (cit. on p. 3).

[6] R. Baxter, *Energy Storage - A Nontechnical Guide*. PennWell, 2007, ISBN: 978-1-59370-072-0 (cit. on p. 3).

[7] S. Koohi-Fayegh and M. A. Rosen, 'A review of energy storage types, applications and recent developments,' *Journal of Energy Storage*, vol. 27, p. 101 047, 2020, ISSN: 2352-152X. DOI: `10.1016/j.est.2019.101047` (cit. on p. 3).

[8] S. Rehman, L. M. Al-Hadhrami and M. M. Alam, 'Pumped hydro energy storage system: A technological review,' *Renewable and Sustainable Energy Reviews*, vol. 44, pp. 586–598, 2015, ISSN: 1364-0321. DOI: `10.1016/j.rser.2014.12.040` (cit. on p. 3).

[9] R. Ansorena Ruiz, L. H. de Vilder, E. B. Prasasti *et al.*, 'Low-head pumped hydro storage: A review on civil structure designs, legal and environmental aspects to make its realization feasible in seawater,' *Renewable and Sustainable Energy Reviews*, vol. 160, p. 112 281, 2022, ISSN: 1364-0321. DOI: `10.1016/j.rser.2022.112281` (cit. on p. 3).

[10] V. Kitsikoudis, P. Archambeau, B. Dewals *et al.*, 'Underground Pumped-Storage Hydropower (UPSH) at the Martelange Mine (Belgium): Underground Reservoir Hydraulics,' *Energies*, vol. 13, no. 14, p. 3512, 2020, ISSN: 1996-1073. DOI: 10.3390/en13143512 (cit. on p. 3).

[11] *ALPHEUS H2020*, URL https://alpheus-h2020.eu/, 2022. (visited on 24th Aug. 2022) (cit. on p. 4).

[12] M. Qudaih, B. Engel, D. Truijen *et al.*, 'The Contribution of Low-Head Pumped Hydro Storage to a successful Energy Transition,' in *Proceedings of the Virtual 19th Wind Integration Workshop*, 2020 (cit. on p. 4).

[13] W. De Boer, F. Verheij, D Zwemmer and R Das, 'The energy island–an inverse pump accumulation station,' *EWEC 2007*, pp. 7–10, 2007 (cit. on p. 4).

[14] H. G. Weller, G. Tabor, H. Jasak and C. Fureby, 'A tensorial approach to computational continuum mechanics using object-oriented techniques,' *Computers in Physics*, vol. 12, no. 6, p. 620, 1998. DOI: 10.1063/1.168744 (cit. on pp. 4, 7).

[15] I. J. Karassik, J. P. Messina, P. Cooper and C. C. Heald, *Pump Handbook, Fourth Edition*. McGraw-Hill Education, 2008, ISBN: 978-0-07-146044-6 (cit. on p. 4).

[16] S. Dixon and C. Hall, *Fluid Mechanics and Thermodynamics of Turbomachinery*, 7th. Butterworth-Heinemann, 2014, ISBN: 978-0-12-415954-9. DOI: 10.1016/C2011-0-05059-7 (cit. on pp. 4, 20).

[17] A. Furukawa, T. Shigemitsu and S. Watanabe, 'Performance test and flow measurement of contra-rotating axial flow pump,' *Journal of Thermal Science*, vol. 16, no. 1, pp. 7–13, 2007, ISSN: 1993-033X. DOI: 10.1007/s11630-007-0007-4 (cit. on p. 4).

[18] OpenCFD, *OpenFOAM - The Open Source CFD Toolbox - User's Guide, version v1912*, OpenCFD Ltd., 2019 (cit. on p. 7).

[19] ——, *OpenFOAM - The Open Source CFD Toolbox - User's Guide, version v2012*, OpenCFD Ltd., 2020 (cit. on p. 7).

[20] F. Menter, 'Two-equation eddy-viscosity turbulence models for engineering applications,' 1994. DOI: 10.2514/3.12149 (cit. on p. 8).

[21] F. Menter and Y. Egorov, 'A scale adaptive simulation model using two-equation models,' in *43rd AIAA aerospace sciences meeting and exhibit*, 2005, p. 1095. DOI: 10.2514/6.2005-1095 (cit. on p. 8).

[22] Y. Egorov and F. Menter, 'Development and Application of SST-SAS Turbulence Model in the DESIDER Project,' in *Advances in Hybrid RANS-LES Modelling*, S.-H. Peng and W. Haase, Eds., Berlin, Heidelberg: Springer, 2008, pp. 261–270, ISBN: 978-3-540-77815-8. DOI: 10.1007/978-3-540-77815-8_27 (cit. on p. 8).

[23] F. R. Menter and Y. Egorov, 'The Scale-Adaptive Simulation Method for Unsteady Turbulent Flow Predictions. Part 1: Theory and Model Description,' *Flow, Turbulence and Combustion*, vol. 85, no. 1, pp. 113–138, 2010, ISSN: 1573-1987. DOI: 10.1007/s10494-010-9264-5 (cit. on p. 8).

[24] H. K. Versteeg and W. Malalasekera, *An introduction to computational fluid dynamics: the finite volume method*, 2nd ed. Pearson Prentice Hall, 2007, ISBN: 1-4058-9104-1 (cit. on p. 9).

[25] H. Jasak, *Error analysis and estimation for the finite volume method with applications to fluid flows*. Imperial College London (University of London), 1996 (cit. on pp. 9, 10).

[26] S. Salehi, H. Nilsson, E. Lillberg and N. Edh, 'An in-depth numerical analysis of transient flow field in a Francis turbine during shutdown,' *Renewable Energy*, vol. 179, pp. 2322–2347, 2021, ISSN: 0960-1481. DOI: 10.1016/j.renene.2021.07.107 (cit. on p. 9).

[27] S. Salehi and H. Nilsson, 'Flow-induced pulsations in Francis turbines during startup - A consequence of an intermittent energy system,' *Renewable Energy*, vol. 188, pp. 1166–1183, 2022, ISSN: 0960-1481. DOI: 10.1016/j.renene.2022.01.111 (cit. on p. 9).

[28] ——, 'Effects of uncertainties in positioning of PIV plane on validation of CFD results of a high-head Francis turbine model,' *Renewable Energy*, 2022, ISSN: 0960-1481. DOI: 10.1016/j.renene.2022.04.018 (cit. on p. 9).

[29] H. Weller, 'Controlling the Computational Modes of the Arbitrarily Structured C Grid,' *Monthly Weather Review*, vol. 140, no. 10, pp. 3220–3234, 2012, ISSN: 1520-0493, 0027-0644. DOI: 10.1175/MWR-D-11-00221.1 (cit. on p. 10).

[30] P. E. Farrell and J. R. Maddison, 'Conservative interpolation between volume meshes by local Galerkin projection,' *Computer Methods in Applied Mechanics and Engineering*, vol. 200, no. 1, pp. 89–100, 2011, ISSN: 0045-7825. DOI: 10.1016/j.cma.2010.07.015 (cit. on p. 10).

[31] H. J. Aguerre, S. Márquez Damián, J. M. Gimenez and N. M. Nigro, 'Conservative handling of arbitrary non-conformal interfaces using an efficient supermesh,' *Journal of Computational Physics*, vol. 335, pp. 21–49, 2017, ISSN: 0021-9991. DOI: 10.1016/j.jcp.2017.01.018 (cit. on p. 10).

[32] M. Beaudoin, H. Nilsson, M. Page, R. Magnan and H. Jasak, 'Evaluation of an improved mixing plane interface for OpenFOAM,' *IOP Conference Series: Earth and Environmental Science*, vol. 22, no. 2, p. 022 004, 2014, ISSN: 1755-1315. DOI: 10.1088/1755-1315/22/2/022004 (cit. on p. 11).

[33] S. V Patankar and D. B Spalding, 'A calculation procedure for heat, mass and momentum transfer in three-dimensional parabolic flows,' *International Journal of Heat and Mass Transfer*, vol. 15, no. 10, pp. 1787–1806, 1972, ISSN: 0017-9310. DOI: 10.1016/0017-9310(72)90054-3 (cit. on p. 11).

[34] E. Robertson, V. Choudhury, S. Bhushan and D. K. Walters, 'Validation of OpenFOAM numerical methods and turbulence models for incompressible bluff body flows,' *Computers & Fluids*, vol. 123, pp. 122–145, 2015, ISSN: 0045-7930. DOI: 10.1016/j.compfluid.2015.09.010 (cit. on p. 11).

[35] F. Municchi, P. P. Nagrani and I. C. Christov, 'A two-fluid model for numerical simulation of shear-dominated suspension flows,' *International Journal of Multiphase Flow*, vol. 120, p. 103 079, 2019, ISSN: 0301-9322. DOI: 10.1016/j.ijmultiphaseflow.2019.07.015 (cit. on p. 11).

[36] R. I Issa, 'Solution of the implicitly discretised fluid flow equations by operator-splitting,' *Journal of Computational Physics*, vol. 62, no. 1, pp. 40–65, 1986, ISSN: 0021-9991. DOI: 10.1016/0021-9991(86)90099-9 (cit. on p. 11).

[37] F. M. White, *Fluid Mechanics*, 8. ed. in SI units. McGraw-Hill, 2016, ISBN: 978-981-4720-17-5 (cit. on pp. 14, 15).

[38] R. Tao, X. Zhou, B. Xu and Z. Wang, 'Numerical investigation of the flow regime and cavitation in the vanes of reversible pump-turbine during pump mode's starting up,' *Renewable Energy*, vol. 141, pp. 9–19, 2019, ISSN: 0960-1481. DOI: 10.1016/j.renene.2019.03.108 (cit. on p. 16).

Appended papers

Paper A

Numerical analysis of an initial design of a counter-rotating pump-turbine

J. Fahlbeck[1], H. Nilsson[1], S. Salehi[1], M. Zangeneh[2], M. Joseph[2]

[1] Department of Mechanics and Maritime Sciences, Chalmers University of Technology, Gothenburg, Sweden
[2] Advanced Design Technology Ltd., London, United Kingdom

IOP Conference Series: Earth and Environmental Science **774** (1) (2021) p. 012066

DOI: 10.1088/1755-1315/774/1/012066

Paper B

Flow Characteristics of Preliminary Shutdown and Startup Sequences for a Model Counter-Rotating Pump-Turbine

J. Fahlbeck, H. Nilsson, S. Salehi

Department of Mechanics and Maritime Sciences, Chalmers University of Technology, Gothenburg, Sweden

Energies **14** (12) (2021) p. 3593

DOI: 10.3390/en14123593

Paper C

A Head Loss Pressure Boundary Condition for Hydraulic Systems

J. Fahlbeck, H. Nilsson, S. Salehi

Department of Mechanics and Maritime Sciences, Chalmers University of Technology, Gothenburg, Sweden

OpenFOAM Journal **2** (2022) pp. 1–12

DOI: 10.51560/ofj.v2.69

Paper D

Evaluation of startup time for a model contra-rotating pump-turbine in pump-mode

J. Fahlbeck, H. Nilsson, S. Salehi

Department of Mechanics and Maritime Sciences, Chalmers University of Technology, Gothenburg, Sweden

IOP Conference Series: Earth and Environmental Science, accepted awaiting publication

Paper E

Surrogate based optimisation of a pump mode startup sequence for a contra-rotating pump-turbine using a genetic algorithm and computational fluid dynamics

J. Fahlbeck, H. Nilsson, S. Salehi

Department of Mechanics and Maritime Sciences, Chalmers University of Technology, Gothenburg, Sweden

Submitted for journal publication, under review